Rainbow-like MoO 3 Nanobelts Fashioned via AFM Micromachining

ARTICLE *in* THE JOURNAL OF PHYSICAL CHEMISTRY C · JANUARY 2010

Impact Factor: 4.77 · DOI: 10.1021/jp908547t

Rainbow-like MoO_3 Nanobelts Fashioned via AFM Micromachining

Y. L. Xie,[†,#] F. C. Cheong,[†,#] Y. W. Zhu,[†,‡,§] B. Varghese,[†,‡] Rajesh Tamang,[†] A. A. Bettiol,[∥,⊥] and C. H. Sow*[,†,‡]

Department of Physics, Blk S12, Faculty of Science, National University of Singapore, 2 Science Drive 3, Singapore 117542, National University of Singapore Nanoscience and Nanotechnology Initiative, 2 Science Drive 3, Singapore 117542, Department of Mechanical Engineering and the Texas Materials Institute, The University of Texas at Austin, One University Station C2200, Austin, Texas 78712-0292, Centre for Ion Beam Applications, Department of Physics, National University of Singapore, Blk S12, 2 Science Drive 3, Singapore 117542, and Engineering Science Programme, Faculty of Engineering, National University of Singapore

Received: September 3, 2009; Revised Manuscript Received: November 3, 2009

Single-crystalline MoO_3 nanobelts were prepared on a wide variety of substrates by a simple evaporation and deposition process using a thermal hot plate. This cost-effective technique has the potential for large-scale production of MoO_3 nanobelts with a unique layered structure. The MoO_3 nanobelts dispersed on silicon substrates exhibited a wide variety of colors attributable to the difference in the thicknesses of the nanobelts. Due to the weak interlayer binding, partial and localized removal of the layered nanobelts was readily achieved via atomic force microscope micromachining, resulting in multicolored patterns on individual nanobelts.

Introduction

One-dimensional metal oxide nanostructures have been actively studied due to their unique properties. Among these nanostructured metal oxides, molybdenum oxide (MoO_3) is a very attractive material and has been used extensively in chemical industry.[1,2] Molybdenum oxide thin films and its nanostructures offer a wide spectrum of potential applications, including field emission devices,[3−5] batteries,[6−9] electrochromic devices,[9−12] gas sensors,[13−16] and catalysts.[1,17−19] Moreover, large-scale synthesis of molybdenum oxide nanostructures is readily achievable using various techniques ranging from direct thermal heating[3] of Mo in a furnace, infrared radiation heating of the Mo foil,[4] and hydrothermal[20,21] and sol−gel methods.[10]

Thermal evaporation of Mo onto substrates is an easy way to synthesize MoO_3 nanostructures. Using Si as substrate, it has been reported by Zhou et al.[3] that, by the thermal evaporation of Mo at ∼1100 °C under the flow of Ar, aligned MoO_3 over a large area can be produced. Li et al.[4] evaporated Mo using infrared radiation heating of Mo in air to a temperature of ∼850 °C and produced nanobelts deposited onto the substrate. Zach et al.[22] have also shown that MoO_3 can be synthesized through the electrodeposition of an alkaline solution of MoO_4^{2-} on graphite using the well-established step-decoration method.

In this work, following our successful application of a hot plate technique to grow nanostructures,[5,23,24] nanomaterials of MoO_3 nanobelts were synthesized via a simple physical vapor deposition approach. It was achieved by placing a substrate over a Mo metal foil, followed by heating using a hot plate in ambient conditions. The direct deposition of MoO_3 nanobelts under ambient conditions on various substrates demonstrated the simplicity, cost effectiveness, and flexibility of this technique. The yield of MoO_3 nanobelts was high for many different types of substrates (glass slide, stainless steel, Au-coated quartz, and steel plate), and as-obtained nanobelts were found to exhibit a wide variety of colors under the observation of an optical microscope.

The colored nanobelts were systematically characterized, with the color spectrum collected using a spectrometer connected to the eyepiece of an optical microscope, and the thickness of the nanobelts was measured using an atomic force microscope (AFM). Armed with the knowledge of the measured thickness for the individual nanobelt, we were able to account for the reflectance and transmission spectrum collected from the spectrometer through Fresnel's equation. Through Fresnel's equation, we calculated the refractive index of the nanobelt to be within the values obtained in thin film MoO_3 and discussed the role of the thickness on the color spectrum.

Finally, with the use of the AFM cantilever, we could controllably scratch away selected portions of an isolated nanobelt and thus were able to locally reduce the thickness of the nanobelt. As a result, we could fashion an individual MoO_3 nanobelt with multiple colors. This is possible because the MoO_3 nanobelt has a layered structure and each layer is held together by weak van der Waals forces.[25] We found that a force of tens of micronewtons was required to perform surface scratching on the nanobelt and the depth of trenches created using this force was of the order of tens of nanometers. The mechanical wearing of the MoO_3 nanobelt surface can be controlled by varying the number of scans and magnitude of the scratching force on the nanobelt. Through the scratching of the nanobelt surface to change the local thickness, multiple-colored nanobelts can be fashioned.

Experimental Section

For the synthesis of the MoO_3 nanobelt, a Mo foil (5 mm × 5 mm × 0.05 mm in size, from Aldrich Chemical Co., Inc.) was used as the Mo source and placed on a Cimarec digital stirring thermal hot plate (see the Supporting Information, Figure

* To whom correspondence should be addressed. E-mail: physowch@nus.edu.sg.
† Faculty of Science, National University of Singapore.
‡ National University of Singapore Nanoscience and Nanotechnology Initiative.
§ The University of Texas at Austin.
∥ Department of Physics, National University of Singapore.
⊥ Faculty of Engineering, National University of Singapore.
# These authors contributed equally to this work.

10.1021/jp908547t
Published on Web 12/07/2009

SI1a). The molybdenum foil was allowed to be heated to a temperature of about 480 °C. A Fisher glass slide was placed on top of the Mo foil (see the Supporting Information, Figure SI1b). The assembly was heated for 2 days before it was naturally cooled to room temperature. The as-grown products were characterized by a scanning electron microscope (SEM, JEOL JSM-6400F), a transmission electron microscope (TEM, JEOL JEM 3010) with built-in energy-dispersive spectroscopy (EDS), a micro-Raman system (Renishaw System 2000, 514 nm excitation), and X-ray diffraction (XRD, Phillips PW 127).

For investigating the optical properties of MoO_3 nanobelts, an n-type silicon substrate was cleaned by sonicating it in isopropanol, rinsing with distilled water, and finally drying with a blower. The top oxide layer of a piece of Mo foil was removed using sandpaper. The foil with the spacer layer (stainless steel with 20 μm × 20 μm grids) and the silicon substrate were placed on a Cimarec digital stirring thermal hot plate. The assembly was heated to a temperature of about 480 °C for 48 h and later cooled naturally to room temperature. MoO_3 nanobelts were deposited on a quartz substrate by drying nanobelts containing ethanol on the quartz substrate. To investigate the color exhibited by each nanobelt, a custom-made eyepiece was fixed to the microscope. The eyepiece with a collimator fixed to one of the ends has a port behind the collimator, allowing the attachment of an optic fiber to collect light reflected of the sample.

To obtain the reflectance spectrum of the colored nanobelt, a reference reflectance spectrum was measured with a standard reflector (STAN-SSH High-reflectivity Specular Reflectance Standard from Ocean Optics) for the halogen light source. The light reflected off the standard reflector was collected by the optical fiber secured to the collimator at the eyepiece, and the light was analyzed using a spectrometer (Ocean Optics HR 4000 high-resolution spectrometer) connected to a computer. To ensure the light collected was from the nanobelt, an aperture was used to narrow the field of view down to just the nanobelts. Calibration of the spectrometer to the light source reflectance spectrum was carried out using the software (SpectraLab) provided with the spectrometer. To obtain the transmission spectrum of the colored nanobelt, a reference transmission spectrum was measured with the quartz substrate without the nanobelts for the halogen light source. The light transmitted through the quartz substrate was collected by the optical fiber secured to the collimator at the eyepiece, and the light was analyzed using the same spectrometer. The exact locations of the nanobelts of interest were noted carefully under the optical microscope. The thicknesses of these nanobelts were acquired using the AFM (Nanoscope IIIa, Digital Instruments) set in tapping mode.

Results and Discussion

The nanostructures were synthesized via direct thermal annealing of the Mo foil under ambient condition. The Mo foil with a Fisher glass slide on top was heated to 480 °C for 2 days before it was cooled to room temperature. The surface of the cooled glass slide facing the Mo foil during heating was found covered with a uniform white translucent film (see the Supporting Information, Figure SI1). Optical micrographs of the deposited thin film revealed layers of rectangular crystallites on the surface of the glass slide (see the Supporting Information, Figure SI1), and around 10% of the total nanobelts synthesized exhibited different colors.

The SEM imaging, Raman spectroscopy studies, and X-ray diffraction analysis of the as-grown products were conducted on the sample on the glass slide. As for the other studies, the glass slide together with the nanostructures was first sonicated in distilled water for 5 min to create an aqueous suspension of nanomaterials. For TEM imaging, a drop of the suspension was left to dry on an Agar Scientific (S166-4) lacey carbon 400 mesh Cu-grid.

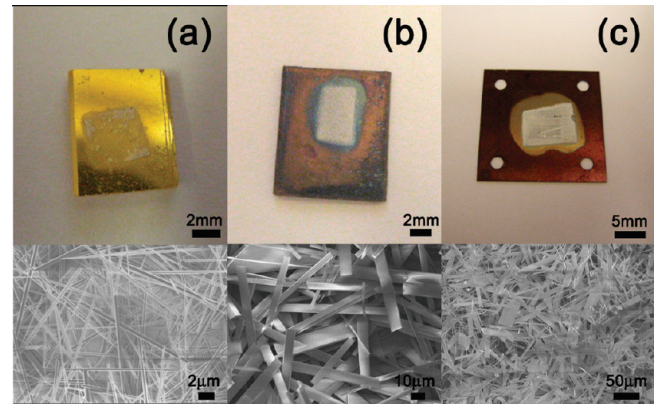

Figure 1. Growth of molybdenum oxide nanobelts on a (a) Au-coated quartz substrate, (b) a steel substrate, and (c) a stainless steel grid substrate Top: images of substrates with nanobelts. Bottom: SEM images of corresponding substrates.

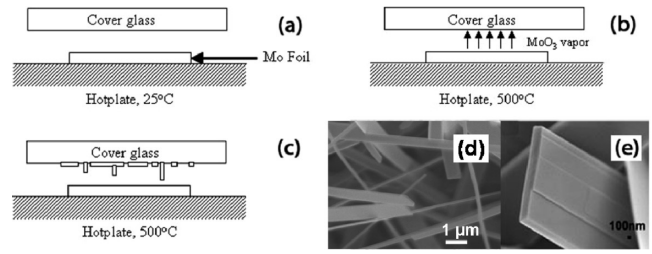

Figure 2. (a−c) Proposed growth mechanism for the MoO_3 nanobelts. (d) MoO_3 nanobelts synthesized on a glass substrate. (e) MoO_3 nanobelts with a layered structure.

One of the advantages of this method is that the nanobelts can be easily synthesized on a wide variety of substrates. Figure 1 shows some examples of successful growth of MoO_3 nanobelts on a Au-coated quartz substrate (Figure 1a), a steel substrate (Figure 1b), and a stainless steel grid substrate (Figure 1c). The morphology of the as-obtained MoO_3 structures was found to be dependent on the substrate. Although nanobelts were formed on all substrates used in this study, Au-coated quartz substrates produced nanobelts with a high aspect ratio. However, the yield of nanobelts on the Au-coated quartz substrate was low compared with the steel, stainless steel, and glass slide substrates. The ability to directly synthesize MoO_3 nanobelts onto different substrates facilitates the ease of device fabrication and sample mounting.

The growth of the MoO_3 nanobelt likely follows a vapor−solid deposition route (Figure 2a−c). Because of continuous heating of the Mo foil surface, surface oxidation at an elevated temperature of about 500 °C (Figure 2b) caused MoO_3 to form on the Mo foil surface. Although the temperature was much lower than the melting point of bulk MoO_3 (912 °C), surface melting was still possible at 500 °C. The Mo oxide became vaporized, carried by the rising hot air, and deposited onto the cooler substrate that was placed directly above the metal foil, as shown in Figure 2b. Furthermore, the temperature gradient existing between the two surfaces of the Mo foil and the substrate favored the deposition of the vapors. This is followed by nucleation and growth of single-crystalline nanobelts along the (001) direction on the glass substrate via a vapor−solid

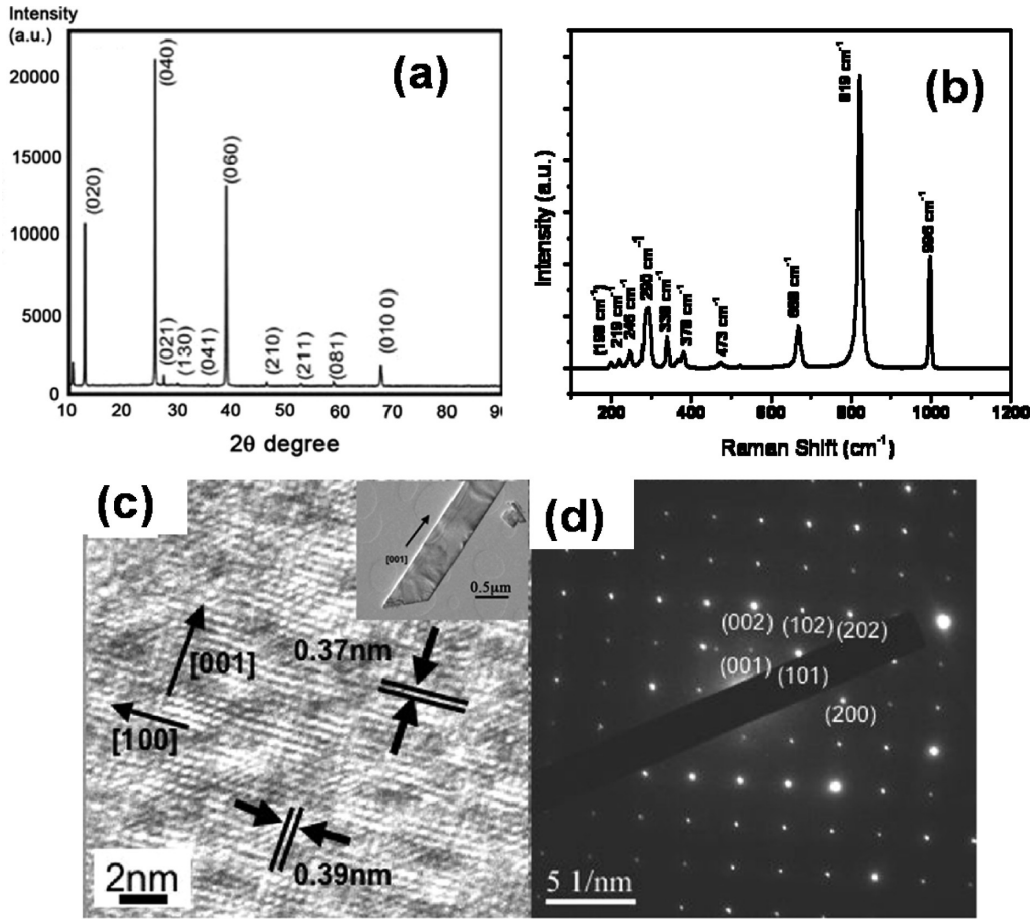

Figure 3. (a) X-ray diffraction pattern and (b) Raman spectrum of the thin film of MoO_3 nanobelts. (c) HRTEM imaging of a MoO_3 nanobelt with the preferential growth direction along [001] (inset: electron micrograph of one MoO_3 nanobelt). (d) Selected area electron diffraction pattern for one MoO_3 nanobelt displaying orthorhombic characteristics.

process (Figure 2c). It should be noted that this growth technique is very user-friendly as MoO_3 can be easily grown on many substrates, such as silicon, silicon with a Au layer, and steel.

Figure 2d shows SEM images of the MoO_3 nanobelts grown on a glass slide. It is evident that uniformly distributed nanobelts had grown over the entire substrate. The nanobelts exhibited a wide range of thicknesses, ranging from 50 to 300 nm; the lengths of the nanobelts were in the range of micrometers and widths of the order of submicrometers. On the other hand, there were hardly any such nanostructures found on the surface of the heated metal foil (see the Supporting Information, Figure SI2). A close-up view of a nanobelt in Figure 2e clearly reveals its layered structure.

The crystal structure of the as obtained products was identified using powder X-ray diffraction (XRD) and micro-Raman spectroscopy. The XRD pattern recorded from a thin film of nanostructures on a cover glass is shown in Figure 3a. All the peaks in the XRD spectrum can be indexed with the orthorhombic structure of MoO_3 phase, with lattice constants $a = 3.96$ Å, $b = 13.86$ Å, and $c = 3.70$ Å (JCPDS card no. 05-0508). The micro-Raman spectrum of the nanobelts, recorded at room temperature, is displayed in Figure 3b. All peaks are in good agreement with the reported orthorhombic MoO_3 single-crystal Raman studies (within the resolution of 2 cm^{-1}) and can be assigned to various vibration modes of the corner shared MoO_6 octahedral basic units.[25] Strong peaks in the range of 600−1000 cm^{-1} correspond to various stretching modes of MoO_6 octahedra (996 cm^{-1} (Mo═O stretching mode), 819 cm^{-1} (Mo−O−Mo stretching modes), and 668 cm^{-1} (triply coordinated oxygen stretching mode)).[26] The peak centered at ∼473 cm^{-1} corresponds to the Mo−O stretching and bending mode of MoO_6 octahedra. Peaks observed in the 400−200 cm^{-1} range (378, 338, 290, 246, 219, and 198 cm^{-1}) correspond to various bending modes of the orthorhombic MoO_3 crystal.

Further characterization was conducted with a high-resolution transmission electron microscope (HRTEM) operating at 300 kV. A typical low-magnification TEM image of the nanobelt is depicted in the inset of Figure 3c. From the HRTEM image (Figure 3c), lattice fringe widths were estimated to be ∼0.39 and 0.37 nm, corresponding to the (100) and (001) plane spacings, respectively, of the orthorhombic MoO_3. In addition, the HRTEM study revealed that the surface of the nanobelts was covered with a thin amorphous layer (see the Supporting

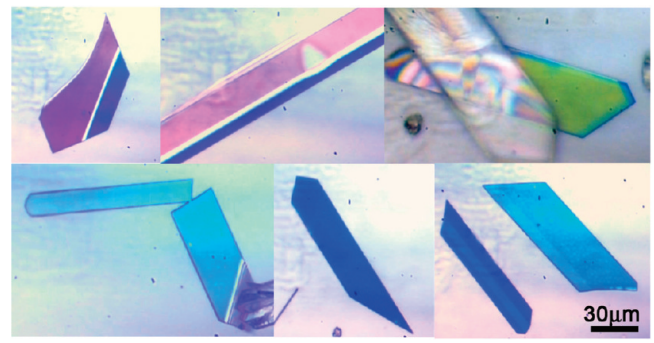

Figure 4. Images of colored MoO_3 nanobelts on a silicon substrate taken from an optical microscope at reflection mode.

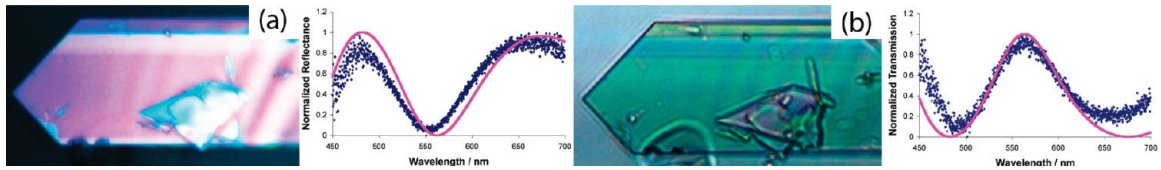

Figure 5. Images of colored MoO_3 nanobelts on a quartz substrate. (a) Reflection mode optical images and the corresponding optical spectrum. (b) Transmission mode optical images and the corresponding optical spectrum. The blue color symbol indicates the experimental value; the red color line indicates the theoretical value.

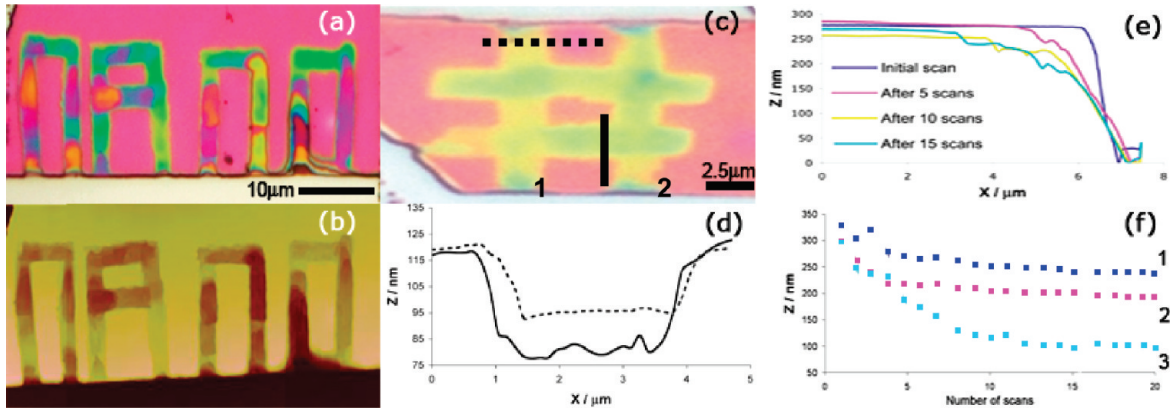

Figure 6. Patterns created by scratching the surface of the MoO_3 with AFM. (a) The word "nano" under an optical microscope. (b) The AFM image of "nano". (c) Hash symbol under an optical microscope. (d) Cross-sectional profile of solid and dashed line in (c), where trench 1 is scratched by 32 μN and trench 2 scratched by 40 μN. (e) Line profile of the edge of the nanobelts during the scratching process. (f) Plot of sample height versus number of scans for different forces (line 1, 11 μN; line 2, 40 μN; line 3, 69 μN).

Information, Figure SI3). The amorphous layer covering on the surface of nanobelts is likely to form during the cooling phase of the growth process. The selected area electron diffraction (SAED) pattern of the nanobelt (Figure 3d) further confirmed its highly crystalline orthorhombic structure with the growth direction along [001].

Under the inspection of an optical microscope, around 10% of the nanobelts was observed to exhibit a rich variety of bright colors (Figure 4). It is well-known that the interference of light in thin films gives rise to colored films.[27] Having lateral dimensions in the micrometer range and thicknesses in the range of 50−400 nm, it is not surprising that the nanobelts exhibit optical properties similar to thin films. Nanobelts that are firmly adhered to the substrate exhibit various colors due to the thickness difference arising from their layered structure. Optical microscope images of the MoO_3 nanobelts displayed in Figure 4 were captured using a CCD camera attached to an optical microscope. With the help of the spectrometer, we were able to obtain the reflectance and transmission spectrum of the colored nanobelts of interest (see the Supporting Information, Figure SI4a). Along with the knowledge of the nanobelt thickness obtained through the height profiling using AFM, the calculation of the reflectance and transmission spectra was calculated through Fresnel's equation. By fitting the experimental data using Fresnel's equation in matrix form acting on a multilayered system[23] (see the Supporting Information, 5), we obtain values of the refractive index, n. From the Fresnel equation, we were able to plot the dispersion curve of the colored MoO_3 nanobelts, which shows that the refractive index n of the nanobelt is not strongly dependent on the wavelength within the visible-light band. Through the dispersion curves, we were able to obtain the average refractive index to be 2.1 ± 0.3. This calculated value is reasonable compared to reported bulk values that vary from 1.8 to 2.45.[28,29] From Figure 5, we can see good agreements for both the experimental and the theoretical spectrum (see the Supporting Information, 5) of the reflection and transmission mode.

Micromachining on individual MoO_3 nanobelts was carried out using an AFM system. The MoO_3 sample was synthesized using the hot plate technique illustrated earlier under a temperature of ~450 °C for 2 days (Figure 1c) on a silicon substrate. After the suitable nanobelt was chosen under the optical microscope, the sample was mounted to the AFM system (Nanoscope IIIa, Digital Instruments). A cantilever with a spring constant of ~60 N m^{-1} was used, and the instrument was initialized in its contact mode. The nanobelt surface was first imaged before additional force was exerted onto the sample surface. When the AFM tip applied a force in the order of 10^{-5} N and scanned across the nanobelt surface, localized mechanical wearing of the nanobelts was observed. This technique facilitates precise control of the location and dimension of the pattern to be created onto the MoO_3 nanobelt surface. This technique is simple to adopt as the scratching process only involves three parameters, mainly the force of the tip acting onto the nanobelt surface, the scanning speed, and the duration of scan. Figure 6a shows an optical image of a MoO_3 nanobelt after performing AFM patterning. All the characters in the word "nano" have straight and well-defined edges. Most importantly, the colors exhibited in the optical micrograph were the result of the interference of light through the MoO_3, which is highly thickness-dependent. The rainbow-like color seen in Figure 6a is the result of nonuniform scratching of the nanobelt surface. The nonuniform scratching causes a difference in the thickness of the nanobelt, and the thickness variation within the nanobelt is illustrated by the AFM image (Figure 6b). Figure 6c shows channels scratched by 2 different forces (~32 μN for trench 1 and ~40 μN for trench 2), which result in different color contrast. Through the use of constant forces and repeated scanning with continuous monitoring of the scratching process until the formation of the pattern, we found that the ~32 μN force created a 25 nm deep trench, whereas the ~40 μN force created a 45 nm trench. The cross-sectional line profile view of the sample elucidates the difference in height profile (Figure 6d).

The ease in scratching the nanobelt surface is attributed to the fact that bilayers of MoO_3 nanobelts were held together by weak van der Waals forces.[25] Figure 6e shows the line profile of the edge of the nanobelt during the scratching process. The onset of scratching was observed to have started from the edge of the nanobelt, and the amount of material scratched away was related to the number of scans. Figure 6f shows how the height of a single point on the nanobelt changes with the number of scans for different tip forces acting on the nanobelt surface. Here, we observed that the depth of scratching increases with increasing force and the reduction in the height of the nanobelt slowly tapers off after repeated scans. Another advantage of using this AFM technique to perform surface manipulation is the effective removal of debris material after the surface had been scratched. This is because, by scanning the surface with a force smaller than the force required for scratching, we were able to sweep the debris to the side of the sample. The ease in the manipulation of the thickness could facilitate the fabrication of sensor devices that are dependent on detector thickness.[30] The observed color spectrum of the MoO_3 nanobelts could be used as a wavelength selector in fiber optics communication or future optoelectronics applications. In addition, the nanobelts could be used as a filter in solar cells to select the wavelength of light essential for photovoltaic (PV) effects to take place.

Conclusions

In conclusion, we have introduced a simple and cost-effective technique to synthesize crystalline MoO_3 nanobelts. One of the advantages of this technique is the ability to grow nanobelts on a wide variety of substrates. The as-prepared MoO_3 nanobelts dispersed on silicon substrates exhibited different colors owing to the difference in their thicknesses. The AFM-based micromachining technique was successfully utilized to remove a localized portion of the individual nanobelts. As a result, individual rainbow-like nanobelts with multiple colors were readily created.

Supporting Information Available: Figures of the thermal hot plate setup, SEM and HRTEM images, and the process to determine the refractive index. This material is available free of charge via the Internet at http://pubs.acs.org.

References and Notes

(1) Ohler, N.; Bell, A. T. *J. Catal.* **2005**, *231*, 115–130.
(2) Fu, G.; Xu, X.; Lu, X.; Wan, H. *J. Phys. Chem. B* **2005**, *109*, 6416–6421.
(3) Zhou, J.; Xu, N. S.; Deng, S. Z.; Chen, J.; She, J. C.; Wang, Z. L. *Adv. Mater.* **2003**, *15*, 1835–1840.
(4) Li, Y. B.; Bando, Y.; Golberg, D.; Kurashima, K. *Appl. Phys. Lett.* **2002**, *81*, 5048–5050.
(5) Zhu, Y. W.; Yu, T.; Cheong, F. C.; Xu, X. J.; Lim, C. T.; Tan, V. B. C.; Thong, J. T. L.; Sow, C. H. *Nanotechnology* **2005**, *16*, 88.
(6) Reddy, C. V. S.; Qi, Y. Y.; Jin, W.; Zhu, Q. Y.; Deng, Z. R.; Chen, W.; Mho, S. I. *J. Solid State Electrochem.* **2007**, *11*, 1239–1243.
(7) Ramirez, I. J.; Martinez-de la Cruz, A. *Mater. Lett.* **2003**, *57*, 1034–1039.
(8) Wen, Z. H.; Wang, Q.; Li, J. H. *J. Nanosci. Nanotechnol.* **2006**, *6*, 2117–2122.
(9) Dillon, A. C.; Mahan, A. H.; Deshpande, R.; Parilla, R.; Jones, K. M.; Lee, S. H. *Metal oxide nano-particles for improved electrochromic and lithium-ion battery technologies*; Elsevier Science Sa: Takayama, Japan, 2006; p 794−797.
(10) Karakurt, I.; Boneberg, J.; Leiderer, P. *Appl. Phys. A: Mater. Sci. Process.* **2006**, *83*, 1–3.
(11) Hsu, C. S.; Chan, C. C.; Huang, H. T.; Peng, C. H.; Hsu, W. C. *Thin Solid Films* **2008**, *516*, 4839–4844.
(12) Mahajan, S. S.; Mujawar, S. H.; Shinde, P. S.; Inamdar, A. I.; Patil, P. S. *Appl. Surf. Sci.* **2008**, *254*, 5895–5898.
(13) Chiorino, A.; Ghiotti, G.; Prinetto, F.; Carotta, M. C.; Gallana, M.; Martinelli, G. *Sens. Actuators, B* **1999**, *59*, 203–209.
(14) Imawan, C.; Solzbacher, F.; Steffes, H.; Obermeier, E. *Gas-sensing characteristics of modified-MoO_3 thin films using Ti-overlayers for NH_3 gas sensors*; Elsevier Science Sa: Sendai, Japan, 1999; p 193−197.
(15) Barazzouk, S.; Tandon, R. P.; Hotchandani, S. *Sens. Actuators, B* **2006**, *119*, 691–694.
(16) Hussain, O. M.; Rao, K. S. *Mater. Chem. Phys.* **2003**, *80*, 638–646.
(17) Wang, F.; Ueda, W. *Chem.—Eur. J.* **2009**, *15*, 742–753.
(18) Paraguay-Delgado, F.; Albiter, M. A.; Huirache-Acuna, R.; Verde, Y.; Alonso-Nunez, G. *Optimization of the synthesis of alpha-MoO_3 nanoribbons and hydrodesulfurization (HDS) catalyst test*; American Scientific Publishers: Arcachon, France, 2006; p 3677−3683.
(19) Meunier, F. C.; Cavallaro, F.; Le Goaziou, T.; Goguet, A.; Rioche, C. *Hydroisomerisation of n-alkanes over partially reduced MoO_3: Promotion by CoAlPO-11 and relations to reaction mechanism and rate-determining step*; Elsevier Science Bv: Louvain la Neuve, Belgium, 2005; p 64−67.
(20) Camacho-Bragado, G. A.; Jose-Yacaman, M. *Appl. Phys. A: Mater. Sci. Process.* **2006**, *82*, 19–22.
(21) Xia, T.; Li, Q.; Liu, X.; Meng, J.; Cao, X. *J. Phys. Chem. B* **2006**, *110*, 2006–2012.
(22) Zach, M. P.; Ng, K. H.; Penner, R. M. *Science* **2000**, *290*, 2120–2123.
(23) Yu, T.; Zhu, Y.; Xu, X.; Yeong, K. S.; Shen, Z.; Chen, P.; Lim, C. T.; Thong, J. T. L.; Sow, C. H. *Small* **2006**, *2*, 80–84.
(24) Yu, T.; Zhu, Y. W.; Xu, X. J.; Shen, Z. X.; Chen, P.; Lim, C. T.; Thong, J. T. L.; Sow, C. H. *Adv. Mater.* **2005**, *17*, 1595–1599.
(25) Chu, W. G.; Zhang, L. N.; Wang, H. F.; Han, Z. H.; Han, D.; Li, Q. Q.; Fan, S. S. *J. Mater. Res.* **2007**, *22*, 1609–1617.
(26) Ding, Q. P.; Huang, H. B.; Duan, J. H.; Gong, J. F.; Yang, S. G.; Zhao, X. N.; Du, Y. W. *J. Cryst. Growth* **2006**, *294*, 304–308.
(27) Diamanti, M. V.; Curto, B. D.; Pedeferri, M. *Color Res. Appl.* **2008**, *33*, 221–228.
(28) Mohamed, S. H.; Kappertz, O.; Ngaruiya, J. M.; Pedersen, T. P. L.; Drese, R.; Wuttig, M. *Thin Solid Films* **2003**, *429*, 135–143.
(29) Cárdenas, R.; Torres, J.; Alfonso, J. E. *Thin Solid Films* **2005**, *478*, 146–151.
(30) Zribi, A.; Knobloch, A.; Tian, W. C.; Goodwin, S. *Sens. Actuators, A* **2005**, *122*, 31–38.

JP908547T